INTERNATIONAL JOURNAL FOR NUMERICAL METHODS IN ENGINEERING
Int. J. Numer. Meth. Engng 2005; **63**:603–629
Published online 11 March 2005 in Wiley InterScience (www.interscience.wiley.com). DOI: 10.1002/nme.1303

A direct finite element implementation of the gradient-dependent theory

Rashid K. Abu Al-Rub and George Z. Voyiadjis*, †

Department of Civil and Environmental Engineering, Louisiana State University, Baton Rouge, LA 70803, U.S.A.

SUMMARY

The enhanced non-local gradient-dependent theories formulate a constitutive framework on the continuum level that is used to bridge the gap between the micromechanical theories and the classical (local) continuum. They are successful in explaining the size effects encountered at the micron scale and in preserving the well-posedeness of the (I)BVP governing the solution of material instability triggering strain localization. This is due to the incorporation of an intrinsic material length scale parameter in the constitutive description. However, the numerical implementation of these theories is not a direct task because of the higher order of the governing equations. In this paper a direct computational algorithm for the gradient approach is proposed. This algorithm can be implemented in the existing finite element codes without numerous modifications as compared to the current numerical approaches (*Int. J. Solids Struct.* 1988; **24**:581–597; *Int. J. Numer. Meth. Engng* 1992; **35**:521–539; *Eng. Comput.* 1993; **10**:99–121; *Dissertation*, 1994; *Int. J. Numer. Meth. Engng* 1996; **39**:2477–2505; *Int. J. Numer. Meth. Engng* 1996; **39**:3731–3755; *Comput. Meth. Appl. Mech. Eng.* 1998; **163**:11–32; *Comput. Meth. Appl. Mech. Eng.* 1998; **163**:33–53; *Euro. J. Mech. – A/Solids* 1999; **18**:939–962; *Int. J. Solids Struct.* 2000; **37**:7481–7499). A predictor–corrector scheme is proposed for the solution of the non-linear algebraic problem from the FEM. The expressions of the continuum and consistent tangent matrices are provided. The method is validated by conducting various numerical tests. As a result, pathological mesh dependence as obtained in finite element computations with conventional continuum models is no longer encountered. Copyright © 2005 John Wiley & Sons, Ltd.

KEY WORDS: gradient theory; length scale; size effect; material instability; FEM

1. INTRODUCTION

A major research direction that has been evolved rapidly as an outgrowth of the necessity to incorporate length scale measures in the classical continuum theories is the development

*Correspondence to: G. Z. Voyiadjis, Department of Civil and Environmental Engineering, Louisiana State University, Baton Rouge, LA 70803, U.S.A.
†E-mail: voyiadjis@eng.lsu.edu

Contract/grant sponsor: Marine Corps Systems Command; contract/grant number: M67854-03-M-6040
Contract/grant sponsor: Air Force Institute of Technology; contract/grant number: F33601-01-P-0343

Received 19 March 2004
Revised 21 July 2004
Accepted 22 December 2004

of numerical techniques where the length scale parameter is used as a localization limiter; i.e. as a means of preserving the well-posedeness and discretization sensitivity in (initial) boundary value problems [(I)BVP] for strain-softening ductile behaviour and damage-softening brittle behaviour. Another research direction is the need for the development of continuum micromechanical-based theories where the length scale parameter is used to capture the size dependence at the micro-scale [1–10].

The physical origin of localization phenomenon and various types of size effects lies at the micro-scale of observation. The material deformation patterns at the micro-scale are heterogeneous, which raise the presence of higher-order gradients [11, 12]. As a result, gradient-dependent theories were introduced. The enhanced gradient-dependent theories formulate a constitutive framework on the continuum level that is used to bridge the gap between the micromechanical theories and the classical continuum theories. Gradient approaches are based on introduction of length scale effects in the constitutive equations by incorporating higher-order gradients (often the first-order gradient and/or the Laplacian) of the deformation kinematic state variables associated with the non-local continuum. The gradient-dependent approach can be simply derived from the non-local theory of Eringen [13], Pijaudier-Cabot and Bazant [14], and Bazant and Pijaudier-Cabot [15].

Aifantis [16, 17] was one of the first to study the gradient regularization in solid mechanics. However, the gradient theory of Aifantis [16, 17] was motivated by localization of softening and its principal aim was to achieve objectivity of continuum modelling and numerical simulations. Other researchers have contributed substantially to the gradient approach with emphasis on numerical aspects of the theory and its implementation in finite element codes: Lasry and Belytschko [1], Aifantis [18], Zbib and Aifantis [19], Comi and Perego [6], and the pioneering work of de Borst and co-workers (e.g. References [2–5, 9] and the references quoted therein). In addition, we should include here the recent works of Ramaswamy and Aravas [7, 8], Wang *et al*. [20], Aifantis *et al*. [21], Bammann *et al*. [22], Ganghoffer *et al*. [23], Oka *et al*. [24], Askes *et al*. [25], Kuhl *et al*. [26], Geers *et al*. [27], Svedberg and Runesson [10], Chen and Wang [28], Di Prisco *et al*. [29], and Askes and Sluys [30]. Gradient thermodynamic damage models were also introduced by Fremond and Nedjar [31], and Voyiadjis *et al*. [32–34]. In addition, extension of the gradient theory to rate-dependent plasticity/damage has been made recently by few authors [20, 21, 24, 33–36]. In the last decade, another class of gradient theories have advocated that the stress tensor of the resulting three-dimensional constitutive equations is an *asymmetric stress tensor*. These theories assume higher-order gradients of the displacement field (e.g. References [37–42]). This group of theories is in fact a particular case of generalized continua, such as *micromorphic continua* [43], or *continua with microstructure* [44], which were all inspired by the pioneering work of the Cosserat brothers [45]. This is not a review paper and therefore the above list of authors represents a sample rather than a comprehensive list. However, a fairly complete review of this type of modelling is given by Abu Al-Rub [46].

The aforementioned gradient plasticity theories has motivated extensive work on the numerical aspects of the gradient-dependent hardening/softening solids since it eliminated the mesh-size dependence of finite element calculations (e.g. References [1–10, 18–27]), and gave reasonable agreements with the size dependence encountered in composite material experiments (e.g. References [39, 47–50]), micro- and nano-indentation experiments (e.g. References [51–60]) as well as with the micro-bend and micro-twist experiments (e.g. References [54, 61–63]). Moreover, the form and magnitude of the length scale parameter in the gradient plasticity theory has been thoroughly discussed by Abu Al-Rub [46] and Abu Al-Rub and Voyiadjis [59, 60]

and Voyiadjis and Abu Al-Rub [63]. They showed that for plasticity deformed polycrystals indentation size effect, micro-torsion, and/or micro-bending results can be used to determine the magnitude of the length scale parameter. Moreover, they used dislocation-based arguments to derive an expression involving the average number of grains through the specimen size, the average spacing between dislocations, and the plastic hardening exponent.

Although gradient-enhanced theories have provided many useful results, there are still difficulties with their numerical implementation, mainly due to the higher order of the governing equations in the inelastic region. For example, the consistency condition of plasticity, through which the plastic multiplier and eventually the plastic strain are calculated, is no longer an algebraic equation but becomes a differential one. Another complication is the higher-order boundary conditions that are necessary from the mathematical point of view and have to be prescribed on the moving elasto-plastic boundary. These internal boundaries are not always easy to interpret physically. The computational technique usually followed for integrating the gradient-dependent constitutive relations was first proposed by de Borst and co-workers (e.g. References [2–5, 9, 64, 65] and the references quoted therein). In their work, the plasticity yield and damage growth conditions depend on the Laplacian of an equivalent kinematic measure (hardening/softening state variables), and the consistency conditions result in differential equations with respect to the plastic/damage multipliers. These multipliers are considered as fundamental unknowns (additional degrees of freedom) having a role similar to that of displacements and are discretized in addition to the usual discretization of the displacements. The consistency condition is written in a weak form and solved simultaneously with the equilibrium equation. Because of the presence of high-order derivatives in the weak form of the (I)BVP, there is a need for numerically expensive C^1-continuous conditions on the shape functions or penalty-enhanced C^0 class functions for the interpolation of the plastic/damage multipliers (or other field variables such as stress and strain) in the finite element context. C^2 and higher continuity are also needed if forth-order or higher-order gradient terms are incorporated, otherwise the gradient terms lose their presence. Therefore, Hermitian or mixed formulations are unavoidable for a consistent finite element formulation. Moreover, for the inelastic process a standard return mapping algorithm is performed, in which the values of the kinematic fields at an integration point are interpolated from their nodal values. This approach has been discussed thoroughly in References [32, 34, 46, 66] and used intensively by many other authors (e.g. References [6–8, 10, 21, 67–72] and the reference quoted therein). The disadvantage of this approach is that it gives rise to many numerical difficulties that require considerable modifications to the existing finite element codes, which makes their implementation not an easy or direct task.

The main purpose of this paper is to formulate a new algorithmic implementation of the gradient-based models. We are looking for an alternative, simple, and robust numerical algorithm for the computation of the higher-order gradient terms without the need for large modifications of existing finite element codes, which makes the gradient approach comparatively easy and attractive to implement in a finite element program. In the approach followed in this paper, the non-local consistency condition is transformed into a linear set of equations that depends on the material parameters and the current co-ordinates of the integration points. These sets of linear equations are solved by any numerical iterative method for the plastic multipliers of the integration points that exist in a global (non-local) superelement of eight adjacent local elements in a non-local sense. The gradient of the effective plastic strain at each integration point in the local element is evaluated from the derivatives of a polynomial that interpolates

the value of the plastic multiplier in the superelement of classical integration points. In this approach there in no need to consider the plastic multiplier as a degree of freedom. Therefore, by using this approach, we do not need to introduce high-order continuous shape functions (e.g. C^1 class or penalty-enhanced C^0 class functions) for the interpolation of the multiplier fields in the finite element. In consequence, a straightforward one-field C^0-continuous finite element implementation can be easily used. Furthermore, this algorithm has the major advantage that it avoids boundary conditions on the moving elasto-plastic boundary since the resulting partial differential equation holds in the whole body. The implementation of the proposed approach is used to simulate strain localization in a two-dimensional specimen subjected to plane strain biaxial compression and a two-dimensional strip in tension. Both exhibit shear banding. The sensitivity of the results to the FEM discretization is in the focus of this paper. The first- and second-order gradients are considered in this work.

The paper is organized as follows: Section 2 summarizes briefly the gradient plasticity theory. Section 3 concentrates on the discretization issues of the gradient-dependent constitutive equations. Section 4 presents the proposed algorithm for computing the gradient terms. The details of the finite element implementation of the proposed algorithm are thoroughly discussed in Section 5. The non-local continuum and consistent tangent stiffnesses are derived in Section 6. Section 7 describes the results of shear band simulations, demonstrating computational robustness in terms of mesh insensitivity. Final conclusions are drawn in Section 8.

2. REVIEW OF GRADIENT-DEPENDENT PLASTICITY

The presentation below is limited to rate-independent elastic–plastic body under static or dynamic loadings. Linear kinematic relations are assumed. The objective is to derive an incremental-iterative algorithm for the gradient-dependent plasticity which satisfies the yield condition in a distributed sense. Unlike the standard algorithms of gradient-dependent plasticity [2–5], the yield condition is satisfied at the end of every loading step similar to that of the equilibrium condition.

The fundamental equations, required for the stress analysis of boundary value problems in elastoplastic solid materials, are outlined as follows. Adapting the standard additive decomposition of strain rates $\dot{\boldsymbol{\varepsilon}}$ into an elastic part $\dot{\boldsymbol{\varepsilon}}^{\mathrm{e}}$ and a plastic part $\dot{\boldsymbol{\varepsilon}}^{\mathrm{p}}$, the stress rate can be written as

$$\dot{\boldsymbol{\sigma}} = \boldsymbol{E} : (\dot{\boldsymbol{\varepsilon}} - \dot{\boldsymbol{\varepsilon}}^{\mathrm{p}}) \tag{1}$$

where $\boldsymbol{\sigma}$ is the Cauchy stress tensor and $\boldsymbol{E}$ is the fourth-order elastic stiffness tensor. The superimposed dot denotes the time derivative of the corresponding field variable. The classical flow rule of associative plasticity is given as

$$\dot{\boldsymbol{\varepsilon}}^{\mathrm{p}} = \dot{\boldsymbol{\lambda}} \boldsymbol{N} \quad \text{with } \boldsymbol{N} = \frac{\partial f}{\partial \boldsymbol{\sigma}} \tag{2}$$

$\dot{\boldsymbol{\lambda}}$ is a non-negative plastic multiplier, $\boldsymbol{N}$ is the gradient to the yield surface f. The yield function f is assumed to be of a von Mises type, such that

$$f = \sqrt{\tfrac{3}{2}\, \boldsymbol{\tau} : \boldsymbol{\tau}} - Y = 0 \tag{3}$$

where $\boldsymbol{\tau}$ is the deviatoric stress tensor and Y is the yield strength. The yield function satisfies the Kuhn–Tucker conditions:

$$\dot{\lambda} \geqslant 0, \quad f \leqslant 0, \quad \dot{\lambda} f = 0 \tag{4}$$

In the classical three-dimensional plasticity of a strain hardening/softening material, the yield strength (Y) is an explicit function of the initial yield strength σ_{yp} and the effective plastic strain p, such that

$$Y = \sigma_{\text{yp}} + hp \tag{5}$$

where h is the hardening/softening modulus. However, in the non-local gradient plasticity theory, p as an internal variable can be replaced by an averaged (non-local) quantity $\widehat{p}$ as follows [14, 15]:

$$\widehat{p}(\boldsymbol{x}) = \frac{1}{V} \int_V \mathbf{h}(\boldsymbol{\zeta}) p(\boldsymbol{x} + \boldsymbol{\zeta}) \, \mathrm{d}V \tag{6}$$

where V is the body volume, $\boldsymbol{x}$ is the point of interest, $\boldsymbol{\zeta}$ is the size of the localized zone, and $\mathbf{h}(\boldsymbol{\zeta})$ is a weighting function which has a unit integral over the whole body volume, and fades away for the points outside the limits of the internal characteristic length scale ℓ. The above integral can be evaluated analytically by expanding $p(\boldsymbol{x} + \boldsymbol{\zeta})$ into a Taylor series around the point $\boldsymbol{x} = 0$. Choosing the error function as the weighting function $\mathbf{h}(\boldsymbol{\zeta})$ and neglecting the higher than second-order terms, the following expression for $\widehat{p}$ can easily be derived as

$$\widehat{p} = p + \ell \|\nabla p\| + \ell^2 \nabla^2 p \tag{7}$$

where $\|\nabla p\|$ is the first-order gradient of p and $\nabla^2 p$ is the second-order (or Laplacian) of p. Most of the studies in the gradient-approach were focused on the role of $\nabla^2 p$ for regularizing the (initial) boundary-value problem (e.g. References [2–6, 9, 10, 18–34, 64–72]). However, there appears to be little reason to consider $\nabla^2 p$ when considering low temperature plasticity [38, 46]. Therefore, both of $\|\nabla p\|$ and $\nabla^2 p$ are considered in this paper. More elaborate results about the role of both $\|\nabla p\|$ and $\nabla^2 p$ are presented by Voyiadjis and Abu Al-Rub [63].

Thus, Equation (5) can now be written as

$$Y = \sigma_{\text{yp}} + h\widehat{p} = \sigma_{\text{yp}} + h(p + \ell \|\nabla p\| + \ell^2 \nabla^2 p) \tag{8}$$

and the non-local von Mises yield function (Equation (3)) is written as follows:

$$f \equiv \sqrt{\tfrac{3}{2} \boldsymbol{\tau} : \boldsymbol{\tau}} - \sigma_{\text{yp}} - h(p + \ell \|\nabla p\| + \ell^2 \nabla^2 p) = 0 \tag{9}$$

For $\ell = 0$ the classical flow theory of plasticity can be retrieved. During plastic flowing, the stress point must remain on the yield surface, that is

$$\dot{f} \equiv \boldsymbol{N} : \dot{\boldsymbol{\sigma}} - h\dot{p} - h\ell \|\nabla \dot{p}\| - h\ell^2 \nabla^2 \dot{p} = 0 \tag{10}$$

Numerical discretization and implementation of the above equations into finite element code (e.g. ABAQUS [73]) is discussed below.

3. DISCRETIZATION OF THE GRADIENT-DEPENDENT CONSTITUTIVE EQUATIONS

For the interval from time t to $t+\Delta t$, the backward Euler method enables the proposed constitutive model (Equations (1) and (2)) to be discretized as follows:

$$\Delta\boldsymbol{\sigma}_{t+\Delta t} = \boldsymbol{E} : (\Delta\boldsymbol{\varepsilon}_{t+\Delta t} - \Delta\lambda_{t+\Delta t}\boldsymbol{N}_{t+\Delta t}) \tag{11}$$

The effective plastic strain at $t+\Delta t$ can be written as

$$p_{t+\Delta t} = p_t + \Delta p_{t+\Delta t} \tag{12}$$

where for a von Mises yield condition (i.e. $\dot{p} = \sqrt{2\dot{\boldsymbol{\varepsilon}}^{\mathrm{p}} : \dot{\boldsymbol{\varepsilon}}^{\mathrm{p}}/3}$), we can write

$$\Delta p_{t+\Delta t} = \Delta\lambda_{t+\Delta t} \quad \text{where } \Delta\lambda_{t+\Delta t} = \int_t^{t+\Delta t} \dot{\lambda}_{t+\Delta t}\,\mathrm{d}t \tag{13}$$

From the above equation, we can write $p_{t+\Delta t}$, $\|\nabla p\|_{t+\Delta t}$, and $\nabla^2 p_{t+\Delta t}$ as

$$p_{t+\Delta t} = p_t + \Delta\lambda_{t+\Delta t} \tag{14}$$

$$\|\nabla p\|_{t+\Delta t} = \|\nabla p\|_t + \|\nabla\Delta\lambda\|_{t+\Delta t} \tag{15}$$

$$\nabla^2 p_{t+\Delta t} = \nabla^2 p_t + \nabla^2\Delta\lambda_{t+\Delta t} \tag{16}$$

Thus, we are seeking to compute $\Delta\lambda_{t+\Delta t}$, $\|\nabla\Delta\lambda\|_{t+\Delta t}$, and $\nabla^2\Delta\lambda_{t+\Delta t}$.

In the following, the elastic predictor–plastic corrector method is adapted as a return mapping algorithm. If the variables at time t, such as $\boldsymbol{\sigma}_t$, $\boldsymbol{\varepsilon}_t$, p_t, are assumed to have been solved and the values of $\Delta\boldsymbol{\varepsilon}_{t+\Delta t}$ and Δt are given, $\boldsymbol{\sigma}_{t+\Delta t}$ that satisfies the discretized constitutive equations can be solved. Therefore, we can write

$$\boldsymbol{\sigma}_{t+\Delta t} = \boldsymbol{E} : (\boldsymbol{\varepsilon}_{t+\Delta t} - \boldsymbol{\varepsilon}^{\mathrm{p}}_{t+\Delta t}) = \boldsymbol{\sigma}^{\mathrm{tr}}_{t+\Delta t} - \Delta\lambda_{t+\Delta t}\boldsymbol{E} : \boldsymbol{N}_{t+\Delta t} \tag{17}$$

where $\boldsymbol{\sigma}^{\mathrm{tr}}_{t+\Delta t}$ is the trial stress tensor and is expressed as

$$\boldsymbol{\sigma}^{\mathrm{tr}}_{t+\Delta t} = \boldsymbol{\sigma}_t + \boldsymbol{E} : \Delta\boldsymbol{\varepsilon}_{t+\Delta t} = \boldsymbol{E} : (\boldsymbol{\varepsilon}^{\mathrm{e}}_t + \Delta\boldsymbol{\varepsilon}_{t+\Delta t}) \tag{18}$$

We can write $\sqrt{\frac{3}{2}\,\boldsymbol{\tau} : \boldsymbol{\tau}} = \sqrt{\frac{3}{2}\,\boldsymbol{\sigma} : \boldsymbol{A} : \boldsymbol{\sigma}}$ and

$$\boldsymbol{N} = \frac{3\boldsymbol{A} : \boldsymbol{\sigma}}{2Y} \tag{19}$$

where $\boldsymbol{A}$ is the conversion matrix from isotropic to deviatoric components and is given by

$$\boldsymbol{A} = \frac{2}{3}\begin{bmatrix} 1 & -\frac{1}{2} & -\frac{1}{2} & 0 & 0 & 0 \\ -\frac{1}{2} & 1 & -\frac{1}{2} & 0 & 0 & 0 \\ -\frac{1}{2} & -\frac{1}{2} & 1 & 0 & 0 & 0 \\ 0 & 0 & 0 & 3 & 0 & 0 \\ 0 & 0 & 0 & 0 & 3 & 0 \\ 0 & 0 & 0 & 0 & 0 & 3 \end{bmatrix} \tag{20}$$

From which, we can rewrite Equation (17) as follows:

$$\boldsymbol{\sigma}_{t+\Delta t} = \boldsymbol{B}_{t+\Delta t} : \boldsymbol{\varepsilon}^{\mathrm{E}}_{t+\Delta t} \tag{21}$$

where $\boldsymbol{B}_{t+\Delta t}$ is the modified elastic tensor and $\boldsymbol{\varepsilon}^{\mathrm{E}}_{t+\Delta t}$ is the modified elastic strain prediction tensor and are given by

$$\boldsymbol{B}_{t+\Delta t} = \left(\boldsymbol{E}^{-1} + \frac{3}{2}\frac{\Delta\lambda_{t+\Delta t}\boldsymbol{A}}{Y_{t+\Delta t}}\right)^{-1} \quad \text{and} \quad \boldsymbol{\varepsilon}^{\mathrm{E}}_{t+\Delta t} = \boldsymbol{\varepsilon}^{\mathrm{e}}_{t} + \Delta\boldsymbol{\varepsilon}_{t+\Delta t} = \boldsymbol{E}^{-1} : \boldsymbol{\sigma}^{\mathrm{tr}}_{t+\Delta t} \tag{22}$$

4. COMPUTATION OF THE GRADIENT PLASTICITY TERMS

In this section, we will show how we can compute the gradient plasticity terms $\|\nabla\Delta\lambda\|$ and $\nabla^2\Delta\lambda$ using a simple and robust approach.

Usually, in the classical plasticity theory, the consistency condition of the yield function is used to determine the current value of the plasticity multiplier $\dot{\lambda}$. Moreover, the unloading/loading condition (Khun–Tucker condition) must be satisfied at each integration point m in the finite element context. However, here the non-local form of the consistency condition, Equation (10), needs some adaptations. A solution is to enforce the consistency condition in the sense of distributions [2–5]. In that case the condition is not satisfied at each iteration but only at the end of the loading step. This approach has been discussed thoroughly by Pamin [4], where he considered the plastic (inelastic) multipliers as independent global variables such that there is a need for C^1 continuous conditions on the shape functions for the interpolation of the plastic (inelastic) multipliers in the finite element context. However, this approach is computationally expensive and large modifications are needed to the finite element code. Therefore, we are looking for a more simple and robust procedure for computation of the gradient plasticity terms.

In the following, we will adapt the above method of enforcing the consistency condition in the sense of distributions; however, the plastic multipliers are not considered here as independent global variables but as local internal variables. Therefore, we do not need to introduce shape functions of the C^1 class or penalty-enhanced C^0 class functions for the interpolation of the plastic multipliers in the finite element.

In classical plasticity, the plastic multiplier is calculated by restoring the consistency condition iteratively. However, for the non-local formulation, it is not possible because it depends on the

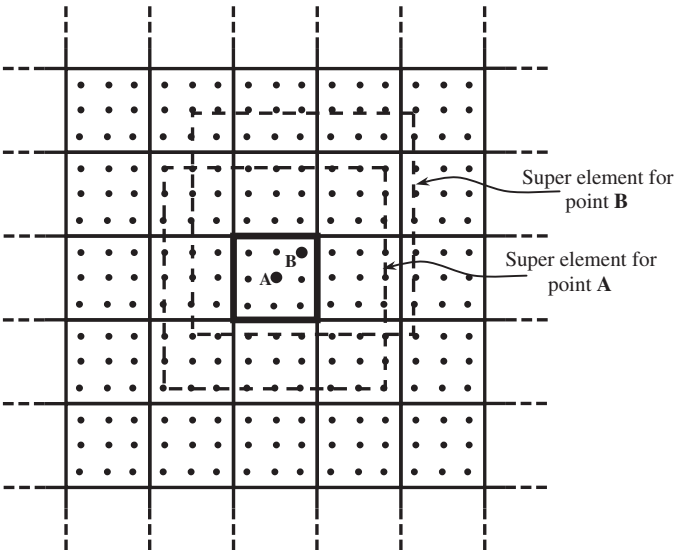

Figure 1. A schematic illustration for the computation of the gradient terms from a regular finite element mesh: Four nodded element with nine integration points with super elements for calculation of the gradient terms.

strain gradient. To evaluate the gradients $\|\nabla\Delta\lambda\|$ and $\nabla^2\Delta\lambda$ at integration point m, we need the values of $\Delta\lambda$ at point m as well as the values at the neighbouring points (non-locality). The gradient at each integration point m is evaluated from the derivatives of a polynomial function that interpolates the values of plastic multiplier at the neighbouring points. Therefore, the gradient terms $\|\nabla\Delta\lambda\|$ and $\nabla^2\Delta\lambda$ can be expressed in terms of $\Delta\lambda_n$ with $n \in \{1, \ldots, N_{\mathrm{GP}}\}$ using the following relation:

$$\|\nabla\Delta\lambda\|_m = \sum_{n=1}^{N_{\mathrm{GP}}} g_{mn}\Delta\lambda_n \tag{23}$$

$$\nabla^2\Delta\lambda_m = \sum_{n=1}^{N_{\mathrm{GP}}} \bar{g}_{mn}\Delta\lambda_n \tag{24}$$

where N_{GP} is the number of Gauss integration points. The computation of coefficients g_{mn} and $\bar{g}_{mn}$ is explained in what follows.

Figure 1 shows a schematic illustration for the computation of the gradient terms from a regular finite element mesh, where the gradient terms are needed at the integration point of each element. For two dimensional problems four nodded element with nine integration points (full integration) is assumed. Eight elements (super element) are used to compute the gradient terms at each integration point. This means that 81 integration points are used to calculate the gradients at each integration point. Except for each corner and mid-boundary elements, their nine integration points are used to calculate the gradients. This illustration is valid for any element with any number of integration points. However, with more integration

points, higher accuracy is achieved in calculating the gradient terms. Moreover, this illustration is valid for one-dimensional as well as for three-dimensional mesh discretizations. However, regular meshes are required and with large precision loss for complicated problems, which limits the applicability of this approach. More elaborate studies are needed to generalize this approach to non-regular mesh discretization.

In order to determine the coefficients g_{mn} and $\bar{g}_{mn}$, a complete second-order polynomial function is used to evaluate the plastic multipliers around point m, such that

$$\Delta\lambda = \boldsymbol{a}^{\mathrm{T}}\boldsymbol{v} \tag{25}$$

where $\boldsymbol{a}$ is the coefficients vector and $\boldsymbol{v}$ is the variables vector. For example in two-dimensional problems we have the following expressions: $\boldsymbol{a}^{\mathrm{T}} = \lfloor a_1 \ a_2 \ a_3 \ a_4 \ a_5 \ a_6 \rfloor$ and $\boldsymbol{v}^{\mathrm{T}} = \lfloor 1 \ x \ y \ xy \ x^2 \ y^2 \rfloor$.

To obtain the coefficients vector $\boldsymbol{a}$, a minimization method by least squares is used. Moreover, the interpolation is made in the global co-ordinate system (x, y, z) of the generated mesh with N_{GP} integration points. The coefficients vector $\boldsymbol{a}$ can be expressed in the following form:

$$\boldsymbol{\Lambda} = \boldsymbol{M}^{\mathrm{T}}\boldsymbol{a} \tag{26}$$

For a two-dimensional mesh the matrix $\boldsymbol{M}$ and the plastic multipliers vector $\boldsymbol{\Lambda}$ are defined by

$$\boldsymbol{M} = \begin{bmatrix} 1 & 1 & \cdots & 1 \\ x_1 & x_2 & \cdots & x_{N_{\mathrm{GP}}} \\ y_1 & y_2 & \cdots & y_{N_{\mathrm{GP}}} \\ x_1 y_1 & x_2 y_2 & \cdots & x_{N_{\mathrm{GP}}} y_{N_{\mathrm{GP}}} \\ x_1^2 & x_2^2 & \cdots & x_{N_{\mathrm{GP}}}^2 \\ y_1^2 & y_2^2 & \cdots & y_{N_{\mathrm{GP}}}^2 \end{bmatrix} \tag{27}$$

and $\boldsymbol{\Lambda} = \lfloor \Delta\lambda_1 \ \Delta\lambda_2 \ \cdots \ \Delta\lambda_{N_{\mathrm{GP}}} \rfloor^{\mathrm{T}}$.

Multiplying both sides of Equation (26) by $\boldsymbol{M}$, we can write

$$\boldsymbol{M}\boldsymbol{\Lambda} = \boldsymbol{H}\boldsymbol{a} \tag{28}$$

with $\boldsymbol{H} = \boldsymbol{M}\boldsymbol{M}^{\mathrm{T}}$ is a symmetrical square matrix and can be written for two-dimensional problems as

$$\boldsymbol{H} = \sum_{n=1}^{N_{\mathrm{GP}}} \begin{bmatrix} 1 & x_n & y_n & x_n y_n & x_n^2 & y_n^2 \\ & x_n^2 & x_n y_n & x_n^2 y_n & x_n^3 & x_n y_n^2 \\ & & y_n^2 & x_n y_n^2 & x_n^2 y_n & y_n^3 \\ & & & x_n^2 y_n^2 & x_n^3 y_n & x_n y_n^3 \\ & \text{Symm} & & & x_n^4 & x_n^2 y_n^2 \\ & & & & & y_n^4 \end{bmatrix} \tag{29}$$

It is obvious that $\boldsymbol{H}$ is computed only one time for small deformation problems and needs to be updated at each loading increment for finite deformation problems.

From Equations (25) and (28), we can compute the plastic multipliers vector and its gradient as follows:

$$\Delta\lambda = \boldsymbol{a}^{\mathrm{T}}\boldsymbol{v} = (\boldsymbol{H}^{-1}\boldsymbol{M}\boldsymbol{\Lambda})^{\mathrm{T}}\boldsymbol{v} = \left(\boldsymbol{H}^{-1}\sum_{n=1}^{N_{\mathrm{GP}}}\Delta\lambda_n\boldsymbol{v}_n\right)^{\mathrm{T}}\boldsymbol{v} \tag{30}$$

$$\nabla\Delta\lambda = \left(\boldsymbol{H}^{-1}\sum_{n=1}^{N_{\mathrm{GP}}}\Delta\lambda_n\boldsymbol{v}_n\right)^{\mathrm{T}}\nabla\boldsymbol{v} \tag{31}$$

For the integration point m, we can write expressions for

$$\|\nabla\Delta\lambda\|_m = \sqrt{(\nabla_x\Delta\lambda_m)^2 + (\nabla_y\Delta\lambda_m)^2 + (\nabla_z\Delta\lambda_m)^2} \tag{32}$$

and

$$\nabla^2\Delta\lambda_m = \nabla_{xx}\Delta\lambda_m + \nabla_{yy}\Delta\lambda_m + \nabla_{zz}\Delta\lambda_m \tag{33}$$

as follows:

$$\|\nabla\Delta\lambda\|_m = \sum_{n=1}^{N_{\mathrm{GP}}}\left(\sqrt{(\boldsymbol{v}_n^{\mathrm{T}}\boldsymbol{H}^{-1}\nabla_x\boldsymbol{v}_m)^2 + (\boldsymbol{v}_n^{\mathrm{T}}\boldsymbol{H}^{-1}\nabla_y\boldsymbol{v}_n)^2 + (\boldsymbol{v}_n^{\mathrm{T}}\boldsymbol{H}^{-1}\nabla_z\boldsymbol{v}_m)^2}\right)\Delta\lambda_n \tag{34}$$

$$\nabla^2\Delta\lambda_m = \sum_{n=1}^{N_{\mathrm{GP}}}(\boldsymbol{v}_n^{\mathrm{T}}\boldsymbol{H}^{-1}\nabla_{xx}\boldsymbol{v}_m + \boldsymbol{v}_n^{\mathrm{T}}\boldsymbol{H}^{-1}\nabla_{yy}\boldsymbol{v}_m + \boldsymbol{v}_n^{\mathrm{T}}\boldsymbol{H}^{-1}\nabla_{zz}\boldsymbol{v}_m)\Delta\lambda_n \tag{35}$$

Comparing Equations (23) and (24) with Equations (34) and (35), respectively, we can then compute the coefficients g_{mn} and $\bar{g}_{mn}$ by

$$g_{mn} = \sqrt{(\boldsymbol{v}_n^{\mathrm{T}}\boldsymbol{H}^{-1}\nabla_x\boldsymbol{v}_m)^2 + (\boldsymbol{v}_n^{\mathrm{T}}\boldsymbol{H}^{-1}\nabla_y\boldsymbol{v}_n)^2 + (\boldsymbol{v}_n^{\mathrm{T}}\boldsymbol{H}^{-1}\nabla_z\boldsymbol{v}_m)^2} \tag{36}$$

$$\bar{g}_{mn} = \boldsymbol{v}_n^{\mathrm{T}}\boldsymbol{H}^{-1}\nabla_{xx}\boldsymbol{v}_m + \boldsymbol{v}_n^{\mathrm{T}}\boldsymbol{H}^{-1}\nabla_{yy}\boldsymbol{v}_m + \boldsymbol{v}_n^{\mathrm{T}}\boldsymbol{H}^{-1}\nabla_{zz}\boldsymbol{v}_m \tag{37}$$

The coefficients g_{mn} and $\bar{g}_{mn}$ depend only on the x, y, z co-ordinates of the Gauss integration points. These coefficients are computed only once for small deformations and at each loading increment for finite deformations.

5. GRADIENT ALGORITHMIC SCHEME

Using Equations (9), (14)–(16), and (21) the non-local yield condition at an integration point m can be expressed using the plastic multipliers by

$$f(\sigma_m, p_m, \|\nabla p\|_m, \nabla^2 p_m) = f(\Delta\lambda_m, \|\nabla\Delta\lambda\|_m, \nabla^2\Delta\lambda_m) = 0 \tag{38}$$

The indication $n+1$ is removed, in order to simplify writing of the equations. Using Equations (23) and (24), we can rewrite the above condition as

$$f(\Delta\lambda_m, \|\nabla\Delta\lambda\|_m, \nabla^2\Delta\lambda_m) = f(\Delta\lambda_m, \{\Delta\lambda_n, n \neq m, n \in \{1, \ldots, N_{\mathrm{GP}}\}\}) = 0 \tag{39}$$

In order to solve this non-linear equation on $\Delta\lambda_m$ and $\Delta\lambda_n$ with $n \in \{1, \ldots, N_{\mathrm{GP}}\}$, we can use the first-order Taylor series expansion of f at the m integration point. The iterative scheme (indication i) at Gauss integration point m and time step $n+1$ can then be written as

$$\begin{aligned} &f(\Delta\lambda_m^{(i+1)}, \{\Delta\lambda_n^{(i+1)}, n \neq m, n \in \{1, \ldots, N_{\mathrm{GP}}\}\}) \\ &\quad = f(\Delta\lambda_m^{(i)}, \{\Delta\lambda_n^{(i)}, n \neq m, n \in \{1, \ldots, N_{\mathrm{GP}}\}\}) \\ &\qquad + \sum_{r=1}^{N_{\mathrm{GP}}} \frac{\partial f(\Delta\lambda_m^{(i)}, \{\Delta\lambda_n^{(i)}, n \neq m, n \in \{1, \ldots, N_{\mathrm{GP}}\}\})}{\partial\Delta\lambda_r} \delta\Delta\lambda_r^{(i+1)} \end{aligned} \tag{40}$$

where

$$\Delta\lambda_r^{(i+1)} = \Delta\lambda_r^{(i)} + \delta\Delta\lambda_r^{(i+1)} \quad \text{with } r \in \{1, \ldots, N_{\mathrm{GP}}\} \tag{41}$$

and

$$\begin{aligned} &f(\Delta\lambda_m^{(i)}, \{\Delta\lambda_n^{(i)}, n \neq m, n \in \{1, \ldots, N_{\mathrm{GP}}\}\}) \\ &\quad = f_m^{(i)} = \sqrt{\tfrac{3}{2}\,\boldsymbol{\sigma}_m^{(i)} : \boldsymbol{A} : \boldsymbol{\sigma}_m^{(i)}} - \sigma_{\mathrm{yp}} - h(p_m^{(i)} + \ell\|\nabla p\|_m^{(i)} + \ell^2\nabla^2 p_m^{(i)}) \end{aligned} \tag{42}$$

The yield function in Equation (39) can be divided into four parts at iteration (i):

$$f(\Delta\lambda_m^{(i)}, \|\nabla\Delta\lambda\|_m^{(i)}, \nabla^2\Delta\lambda_m^{(i)}) = f_1(\Delta\lambda_m^{(i)}) - f_2(\Delta\lambda_m^{(i)}) - f_3(\|\nabla\Delta\lambda\|_m^{(i)}) - f_4(\nabla^2\Delta\lambda_m^{(i)}) = 0 \tag{43}$$

with

$$f_1(\Delta\lambda_m^{(i)}) = \sqrt{\tfrac{3}{2}\,\boldsymbol{B}_m^{(i)} : \boldsymbol{\varepsilon}_m^{\mathrm{E}} : \boldsymbol{A} : \boldsymbol{B}_m^{(i)} : \boldsymbol{\varepsilon}_m^{\mathrm{E}}} \tag{44}$$

where $\boldsymbol{B}_m$ is a function of $\Delta\lambda_m^{(i)}$;

$$f_2(\Delta\lambda_m^{(i)}) = h(p_m + \Delta\lambda_m^{(i)}) \tag{45}$$

$$f_3(\|\nabla\Delta\lambda\|_m^{(i)}) = h\ell(\|\nabla p\|_m + \|\nabla\Delta\lambda\|_m^{(i)}) = h\ell \sum_{n=1}^{N_{\mathrm{GP}}} g_{mn}(p_n + \Delta\lambda_n^{(i)}) \tag{46}$$

$$f_4(\nabla^2\Delta\lambda_m^{(i)}) = h\ell^2(\nabla^2 p_m + \nabla^2\Delta\lambda_m^{(i)}) = h\ell^2 \sum_{n=1}^{N_{\mathrm{GP}}} \bar{g}_{mn}(p_n + \Delta\lambda_n^{(i)}) \tag{47}$$

The derivatives in Equation (40) can then be written as

$$\frac{\partial f_1(\Delta\lambda_m^{(i)})}{\partial\Delta\lambda_n} = -\boldsymbol{\delta}_{mn} : \boldsymbol{N}_m^{(i)} : \boldsymbol{B}_m^{(i)} : \boldsymbol{N}_m^{(i)} \tag{48}$$

$$\frac{\partial f_2(\Delta\lambda_m^{(i)})}{\partial \Delta\lambda_n} = h\delta_{mn} \tag{49}$$

$$\frac{\partial f_3(\|\nabla\Delta\lambda\|_m^{(i)})}{\partial \Delta\lambda_n} = h\ell g_{mn} \tag{50}$$

$$\frac{\partial f_4(\nabla^2\Delta\lambda_m^{(i)})}{\partial \Delta\lambda_n} = h\ell^2 \bar{g}_{mn} \tag{51}$$

where δ_{mn} is equal to 1 when $m = n$ else it is 0, and $\boldsymbol{N}_m^{(i)}$ is given by

$$\boldsymbol{N}_m^{(i)} = \frac{3}{2} \frac{\boldsymbol{A} : \boldsymbol{\sigma}_m^{(i)}}{\sqrt{\frac{3}{2}\, \boldsymbol{\sigma}_m^{(i)} : \boldsymbol{A} : \boldsymbol{\sigma}_m^{(i)}}} \tag{52}$$

Now, we can write the consistency condition in Equation (40) at Gauss integration point m from Equations (42) and (48)–(51) as follows:

$$f_m^{(i)} - (\boldsymbol{N}_m^{(i)} : \boldsymbol{B}_m^{(i)} : \boldsymbol{N}_m^{(i)} + h)\delta\Delta\lambda_m^{(i+1)} - h\ell \sum_{n=1}^{N_{\mathrm{GP}}} (g_{mn} + \ell \bar{g}_{mn})\delta\Delta\lambda_n^{(i+1)} = 0 \tag{53}$$

Let us define the following expressions:

$$R_m^{(i)} = \boldsymbol{N}_m^{(i)} : \boldsymbol{B}_m^{(i)} : \boldsymbol{N}_m^{(i)} + h \tag{54}$$

$$\boldsymbol{G}^{(i)} = \begin{bmatrix} R_1^{(i)} + h\ell(g_{11} + \ell\bar{g}_{11}) & h\ell(g_{12} + \ell\bar{g}_{12}) & \cdots & h\ell(g_{1N_{\mathrm{GP}}} + \ell\bar{g}_{1N_{\mathrm{GP}}}) \\ h\ell(g_{21} + \ell\bar{g}_{21}) & R_2^{(i)} + h\ell(g_{22} + \ell\bar{g}_{22}) & \cdots & h\ell(g_{2N_{\mathrm{GP}}} + \ell\bar{g}_{2N_{\mathrm{GP}}}) \\ \vdots & \vdots & \vdots\ddots & \vdots \\ h\ell(g_{N_{\mathrm{GP}}1} + \ell\bar{g}_{N_{\mathrm{GP}}1}) & h\ell(g_{N_{\mathrm{GP}}2} + \ell\bar{g}_{N_{\mathrm{GP}}2}) & \cdots & R_{N_{\mathrm{GP}}}^{(i)} + h\ell(g_{N_{\mathrm{GP}}N_{\mathrm{GP}}} + \ell\bar{g}_{N_{\mathrm{GP}}N_{\mathrm{GP}}}) \end{bmatrix} \tag{55}$$

$$\delta\boldsymbol{\Lambda}^{(i+1)} = \lfloor \delta\Delta\lambda_1^{(i+1)} \;\; \delta\Delta\lambda_2^{(i+1)} \;\; \cdots \;\; \delta\Delta\lambda_{N_{\mathrm{GP}}}^{(i+1)} \rfloor^{\mathrm{T}} \tag{56}$$

$$\boldsymbol{f}^{(i)} = \lfloor f_1^{(i)} \;\; f_2^{(i)} \;\; \cdots f_{N_{\mathrm{GP}}}^{(i)} \rfloor^{\mathrm{T}} \tag{57}$$

Then we can express the iterative system of Equation (53) in a matrix format at time $t + \Delta t$ by

$$\boldsymbol{G}^{(i)}\boldsymbol{\delta\Lambda}^{(i+1)} = \boldsymbol{f}^{(i)} \tag{58}$$

The above linear-system of equations can be solved for $\boldsymbol{\delta\Lambda}^{(i+1)}$, using a numerical iterative method such as the Gauss–Jordan iterative scheme. The plastic multipliers are obtained for the minimum of ERROR $\leqslant$ TOL such that

$$\mathrm{ERROR} = \sum_{n=1}^{N_{\mathrm{GP}}} (\lambda_n^{(i+1)} - \lambda_n^{(i)})^2 \tag{59}$$

where TOL is an error tolerance which could be set to a very small value in the order of 10^{-10}.

6. NON-LOCAL GRADIENT-DEPENDENT TANGENT MODULI

In the following, the non-local elastoplastic tangent stiffness $\boldsymbol{D}^{\mathrm{ep}}_{t+\Delta t} = \Delta\boldsymbol{\sigma}_{t+\Delta t}/\Delta\boldsymbol{\varepsilon}_{t+\Delta t}$ between time t and $t+\Delta t$ will be derived for the above constitutive equations. The consistency $\Delta f_{t+\Delta t}$ condition can be written at integration point m as

$$\Delta f_m \equiv \frac{\partial f}{\partial \boldsymbol{\sigma}_m}\Delta\boldsymbol{\sigma}_m + \frac{\partial f}{\partial p_m}\Delta p_m + \frac{\partial f}{\partial \|\nabla p\|_m}\|\nabla\Delta p\|_m + \frac{\partial f}{\partial \nabla^2 p_m}\nabla^2\Delta p_m = 0 \tag{60}$$

Substituting Equations (9), (11), (13), (23), and (24) into the above consistency condition, we can obtain a closed form expression for the plasticity multiplier $\Delta\lambda_m$ at integration point m as

$$\Delta\lambda_m = \left\langle \frac{1}{H_m}\boldsymbol{N}_m : \boldsymbol{E} : \Delta\boldsymbol{\varepsilon}_m \right\rangle \tag{61}$$

Note that the indication $t+\Delta t$ is removed for clarity. H_m is the non-local hardening modulus at integration point m and is given by

$$H_m = \boldsymbol{N}_m : \boldsymbol{E} : \boldsymbol{N}_m + h(1 + \ell g_{mm} + \ell^2 \bar{g}_{mm}) + \frac{h\ell}{\Delta\lambda_m}\sum_{n=1,\, m\neq n}^{N_{\mathrm{GP}}} g_{mn}\Delta\lambda_n + \frac{h\ell^2}{\Delta\lambda_m}\sum_{n=1,\, m\neq n}^{N_{\mathrm{GP}}} \bar{g}_{mn}\Delta\lambda_n \tag{62}$$

The elasto-plastic tangent stiffness at integration point m, $\boldsymbol{D}^{\mathrm{ep}}_m$, is defined by Equation (11) along with Equation (61), such that

$$\boldsymbol{D}^{\mathrm{ep}}_m = \boldsymbol{E} - \frac{1}{H_m}(\boldsymbol{N}_m : \boldsymbol{E} \otimes \boldsymbol{E} : \boldsymbol{N}_m) \tag{63}$$

where $\otimes$ represents the dyadic tensor product. If we set $\ell = 0$ then we retain the local elasto-plastic tangent stiffness matrix.

However, to preserve the quadratic convergence of the rate of Newton–Raphson method, small time increments are used or we can use the non-local consistent (algorithmic) tangent modulus. For this purpose we differentiate Equation (11) at integration point m as

$$\mathrm{d}\Delta\boldsymbol{\sigma}_m = \boldsymbol{E} : (\mathrm{d}\Delta\boldsymbol{\varepsilon}_m - \mathrm{d}\Delta\lambda_m\boldsymbol{N}_m - \Delta\lambda_m\mathrm{d}\boldsymbol{N}_m) \tag{64}$$

Using the chain rule, we can rewrite the above equation as

$$\mathrm{d}\Delta\boldsymbol{\sigma}_m = \boldsymbol{E} : \left(\mathrm{d}\Delta\boldsymbol{\varepsilon}_m - \left(\frac{\partial\Delta\lambda_m}{\partial\Delta\boldsymbol{\varepsilon}_m} : \mathrm{d}\Delta\boldsymbol{\varepsilon}_m\right)\boldsymbol{N}_m - \Delta\lambda_m\frac{\partial\boldsymbol{N}_m}{\partial\Delta\boldsymbol{\varepsilon}_m} : \mathrm{d}\Delta\boldsymbol{\varepsilon}_m\right) \tag{65}$$

or equivalently we can rewrite the above expression as

$$\mathrm{d}\Delta\boldsymbol{\sigma}_m = \boldsymbol{D}^{\mathrm{alg}}_m : \mathrm{d}\Delta\boldsymbol{\varepsilon}_m \tag{66}$$

where $\boldsymbol{D}_m^{\text{alg}}$ is the algorithmic tangent modulus and is given by

$$\boldsymbol{D}_m^{\text{alg}} = \boldsymbol{E} - (\boldsymbol{E} : \boldsymbol{N}_m) \otimes \frac{\partial \Delta\lambda_m}{\partial \Delta\boldsymbol{\varepsilon}_m} - \Delta\lambda_m \left(\boldsymbol{E} : \frac{\partial \boldsymbol{N}_m}{\partial \Delta\boldsymbol{\varepsilon}_m} \right) \tag{67}$$

We can simply find an expression for $\partial\Delta\lambda/\partial\Delta\boldsymbol{\varepsilon}$ and $\partial\boldsymbol{N}/\partial\Delta\boldsymbol{\varepsilon}$ by combining Equations (11), (19), and (61), such that

$$\frac{\partial \Delta\lambda}{\partial \Delta\boldsymbol{\varepsilon}} = \frac{1}{H} \left(\boldsymbol{E} : \boldsymbol{N} + \frac{\partial \boldsymbol{N}}{\partial \Delta\boldsymbol{\varepsilon}} : \boldsymbol{E} : \Delta\boldsymbol{\varepsilon} \right) \tag{68}$$

$$\frac{\partial \boldsymbol{N}}{\partial \Delta\boldsymbol{\varepsilon}} = \frac{3}{2Y} \boldsymbol{A} : \left(\boldsymbol{E} - \frac{1}{H} (\boldsymbol{E} : \boldsymbol{N}) \otimes (\boldsymbol{N} : \boldsymbol{E}) \right) \tag{69}$$

Substituting Equations (68) and (69) into Equation (67) yields

$$\boldsymbol{D}_m^{\text{alg}} = \boldsymbol{D}_m^{\text{ep}} - \frac{3}{2Y_m} \boldsymbol{D}_m^{\text{ep}} : \boldsymbol{A} : \left(\Delta\lambda_m \boldsymbol{E} + \frac{1}{H_m} (\boldsymbol{E} : \boldsymbol{N}_m) \otimes (\boldsymbol{E} : \Delta\boldsymbol{\varepsilon}) \right) \tag{70}$$

For large loading steps the second operator $\boldsymbol{D}^{\text{alg}}$ differs significantly from the continuous operator $\boldsymbol{D}^{\text{ep}}$. However, the way in which the element tangent stiffness matrix is constructed must be consistent with the algorithmic relationship between the stress increment and the strain increment.

For convenience, a step-by-step description of the algorithm discussed above is illustrated in the flow diagram in Figure 2. The algorithm in Figure 2 can also be used for gradient-independent plasticity by setting the value of the length scale parameter ℓ to zero.

Note that an integration point m is assumed to be in the plastic state when $f_m > 0$ and in the elastic state when $f_m < 0$. In the elastic elements $\Delta\lambda_m = 0$; however, for spreading of the plastic zone it is important that the numerical solution allows $\|\nabla\Delta\lambda_m\| > 0$ and/or $\nabla^2\Delta\lambda_m > 0$ at the elastic–plastic boundary. The non-local yield strength Y_m is then increased/decreased (depending on the sign of the length scale parameter, ℓ, in Equation (8) with negative-decreasing and positive-increasing) as a result of the hardening/softening process in the neighbourhood.

Moreover, for the elastic state we set the residual force $\boldsymbol{f}$ to zero. Equation (58) yields the desired solution $\delta\boldsymbol{\Lambda} = 0$ if the global matrix $\boldsymbol{G}$ is non-singular. However, if plastic integration points appear in the structure, then in the elastic integration points adjacent to the plastic zone we have $\boldsymbol{f} \neq 0$ and we have non-zero $\delta\boldsymbol{\Lambda}$ from Equation (58). The proposed algorithm has the feature, that these elastic integration points have $\Delta\lambda \approx 0$ and $\|\nabla\Delta\lambda_m\| > 0$ and $\nabla^2\Delta\lambda_m > 0$. As a result the yield strength Y is increased/decreased and the plasticity at these elastic points is delayed (hardening) or enters the plastic region (softening).

It should be also noted that it is unnecessary in the proposed approach to input the value of h in Equation (55) to a large value in order to constrain the value of $\Delta\lambda$ to zero for the elastic integration points as had been suggested by de Borst and Mühlhaus [2]. In fact, this substitution adversely affects the accuracy of the local return mapping and for some integration points it may cause containment of the plastic flow in the initially imperfect zones and prevent the regularization effect. In this study an artificial value of h is taken equal to the Young's modulus for integration points in the elastic state and substituted in the matrix $\boldsymbol{G}$ to avoid singularity.

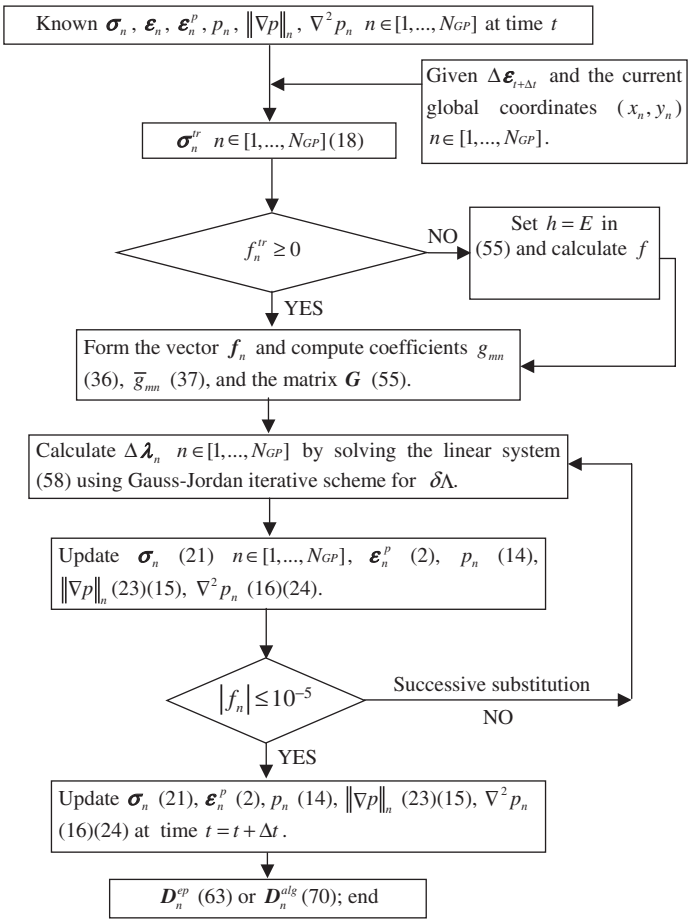

Figure 2. Flow chart of the proposed stress integration algorithm for gradient-dependent plasticity theory.

Moreover, the yield condition, Equation (9), is not satisfied until convergence is achieved. It can happen that due to stress redistribution or non-linear softening that $\Delta\lambda_m$ results in a return mapping to the inside of the yield surface. In the present computational algorithm this does not cause the detection of unloading, but changes sign of the residual forces $\boldsymbol{f}$, which results further in a proper correction (decrease) of $\Delta\lambda_m$.

Due to introduction of additional gradients of the effective plastic strain into the yield function, we need to add suitable boundary conditions for the uniqueness of solution (see References [4, 46]). In the elastic–plastic boundary (S_{ep}), as we mentioned earlier, the effective (equivalent) plastic strain vanishes,

$$p = 0 \quad \text{for } \boldsymbol{x}_i \to S_{\text{ep}} \tag{71}$$

Should the plastic zone spread over specimen boundaries, Mühlhaus and de Borst [2] suggested to introduce

$$\frac{\partial p}{\partial \boldsymbol{n}} = 0 \quad \text{for } \boldsymbol{x}_i \to S_p \tag{72}$$

as an additional boundary condition for all plastic boundaries (S_p) with $\boldsymbol{n}$ being the outward normal vector on the plastic surface S_p. Pamin [4] stated that this condition is not enough to avoid the singular stiffness matrix, where he added

$$\frac{\partial^2 p}{\partial \boldsymbol{n} \partial \boldsymbol{m}} = 0 \quad \text{for } \boldsymbol{x}_i \to S_p \tag{73}$$

as the additional boundary to suppress the system singularity with $\boldsymbol{m}$ being the tangent vector of the plastic boundary S_p.

The elastic–plastic boundary of a specimen is unknown during the loading increment (or iteration). We can therefore set this boundary condition to the whole specimen boundaries. In the numerical examples considered in the next section, these boundary conditions of the proposed approach are trivial and do not affect the solutions. Therefore, compared to the well-known numerical algorithm presented by de Borst and co-workers for the gradient approach, the algorithm in this paper has the major advantage that it avoids boundary conditions on the moving elasto-plastic boundaries.

The above algorithm for gradient-dependent plasticity appears to have several advantages over the standard algorithm by de Borst and his co-workers with regard to the incorporation of the gradient-dependent plasticity model. The proposed computational algorithm can be implemented in the existing finite element codes without large modifications as compared to the computational approach of de Borst and his co-workers. In contrast to the later approach, for calculation of the gradient terms we do not need to introduce shape functions of the C^1 class or penalty-enhanced C^0 class functions [2–10, 32] for the interpolation of the effective plastic (inelastic) strain and the gradient terms. This is because the governing constitutive equations in the proposed approach are replaced directly by the difference equations of the field variables and no interpolation functions are needed for the effective plastic strain and the gradient terms.

Finally, it should be emphasized that, if no distinction is made between the rate of small strain $\dot{\boldsymbol{\varepsilon}}$ and the non-linear kinematic term $\boldsymbol{d}$, the above described gradient-dependent algorithm can be used in a finite deformation context. Thus, the above procedure provides a material-independent prescription for extending small-strain updates into finite deformation range within the framework of a hypoelastic formulation. However, we should note that the gradient terms should be calculated in the current configuration if finite strain assumptions are employed.

7. SHEAR BANDING EXAMPLES

We notice that in the absence of a physically motivated length scale which would govern the width of the shear band, such a scale is introduced in the problem by the mesh size. Therefore, in order to remedy the spurious mesh sensitivity of the numerical results an internal length scale is incorporated in the continuum description. The following examples will demonstrate the potential of the gradient computational approach presented in the previous sections in

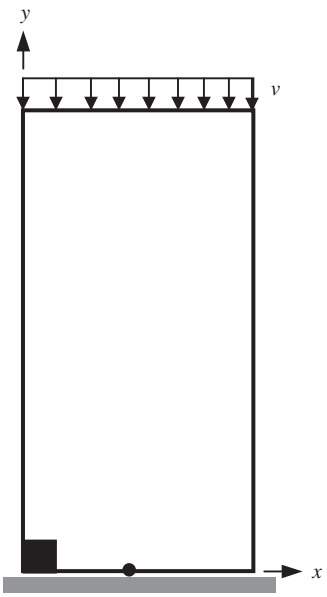

Figure 3. Biaxial compression test configuration (with dimensions $B \times H$ and an imperfection in the bottom left-hand corner).

solving the mesh sensitivity problem. The gradient computational algorithm is implemented in the special purpose user subroutine UMAT in the environment of the ABAQUS/Standard. For details about how to write a UMAT subroutine and implementing it in ABAQUS consult ABAQUS [73].

7.1. Biaxial compression

The spurious mesh dependence of finite element predictions can be illustrated by the example of a simple plane strain specimen in biaxial compression (Figure 3). The specimen is placed on a smooth rigid plane and its upper edge is constrained to remain horizontal (i.e. smooth rigid plate is placed at the top) while a vertical deformation equivalent to a compressive force is applied (see Figure 3). The central point of the bottom plate is fixed to avoid rigid body displacement. The forces per unit area at both sides of the specimen are set to zero. Their horizontal displacements as well as the external additional double forces per unit area are assumed to be zero all along the boundaries.

First, the standard plasticity model presented in Section 2 with $\ell = 0$ is used. Three meshes with 15×30, 30×60, and 45×90 with selectively integrated eight-noded elements and 3×3 integration points (full integration) are used. In the calculations we use $H = 60$ mm, $B = 30$ mm, Young's modulus $E = 187$ GPa, the tensile strength $\sigma_{\text{yp}} = 122.5$ MPa, the Poisson's ratio $v = 0.49$, and the softening modulus $h = 0.1E$. To initiate a shear band an area in the bottom left-hand corner of the sample is assigned a slightly lower yield strength σ_{yp} (10% reduction) and the imperfect area is the same for each mesh ($4 \times 4\,\text{mm}^2$). A 1 mm displacement

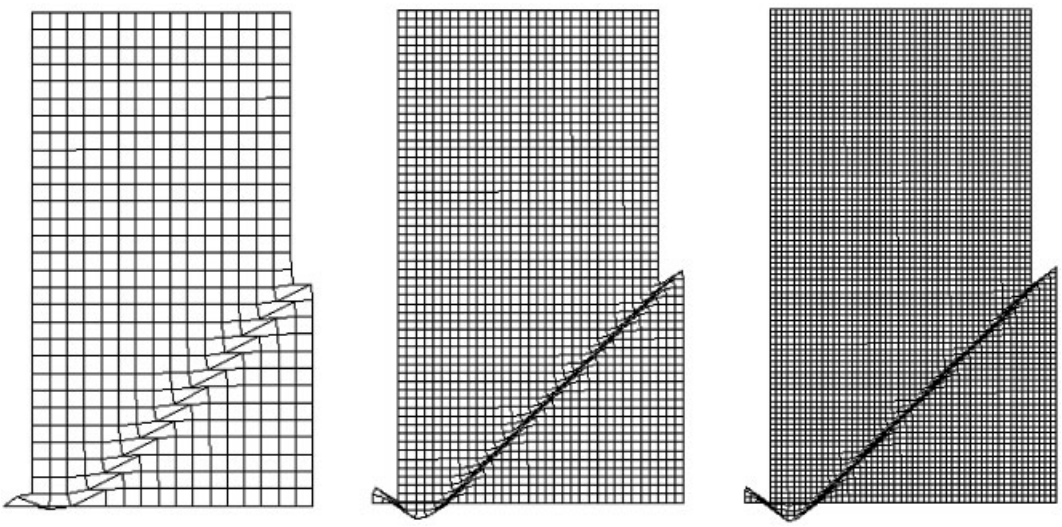

Figure 4. Mesh-dependent results for 15×30, 30×60, and 45×90 meshes. Mesh dependence of deformation patterns for classical continuum of $\ell = 0$ (non-physical response; the finer the mesh the smaller the band width).

is imposed at the top. This benchmark example has been considered by Pamin [4]. Figure 4 shows that the shear band always occupies the smallest possible area. Upon mesh refinement localization in a line is approached, which is not realistic. Moreover, Figure 5 shows plots of the effective plastic strain for the considered meshes. It can be seen that different values are obtained for different meshes, which is also not realistic.

Now, if we repeat the calculations using an internal length scale $\ell = 2.5\,\text{mm}$, mesh objective results are obtained (see Figures 6 and 7). Figure 6 presents the deformation patterns. From this figure it can be checked that the observed width of the shear band is intrinsic and independent of the mesh size. Figure 7 presents contour plots of equal effective plastic strain values for the different discretizations.

It should be also emphasized that, contrary to many researchers showing such patterns (e.g. References [3, 4]), the displacements in Figure 6 are not magnified. The inclusion of geometric non-linearity is important in order to obtain realistic deformation patterns.

7.2. Strip in tension

In the previous example, the evolution of the shear band in a plane biaxial compression test with strain-softening gradient plasticity is investigated and the capability of the gradient theory in providing the mesh objective results is demonstrated. Now, the simulation of a strip in tension as shown in Figure 8 is carried out. The strip is constrained at the bottom, while a displacement of 0.06 mm is imposed at the top. In the calculations we use the Young's modulus $E = 20\,\text{GPa}$, the tensile strength $\sigma_{\text{yp}} = 20\,\text{MPa}$, the Poisson's ratio $\nu = 0.3$, and the softening modulus $h = 0.25E$. Two meshes (mesh1 : 10×20, mesh2 : 20×40) are used with a four-noded quadrilateral plane-strain element. To avoid a homogenous solution, we slightly

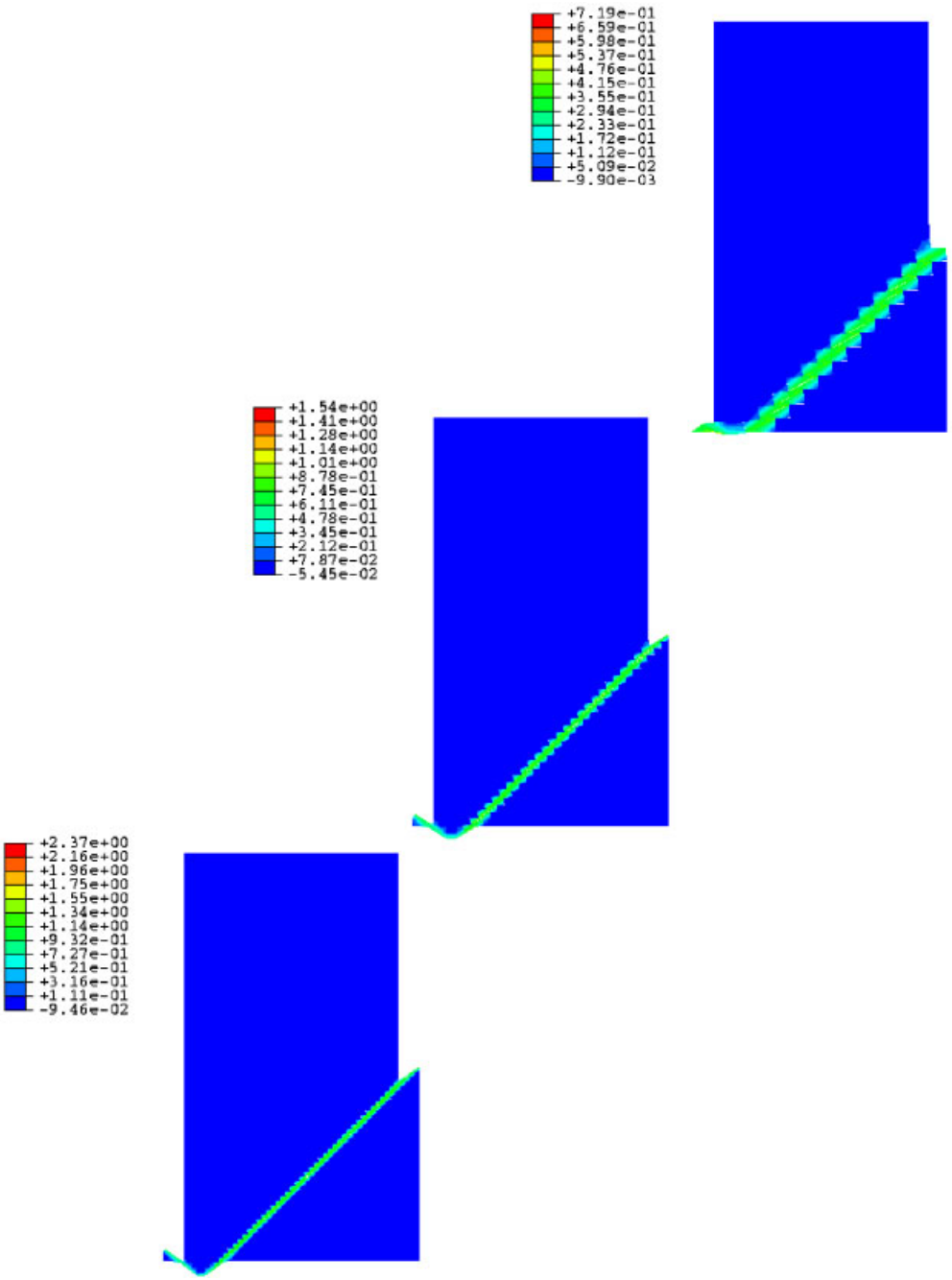

Figure 5. Mesh-sensitivity results for 15×30, 30×60, and 45×90 meshes. Mesh dependence of effective plastic strain contours for classical continuum of $\ell = 0$ (non-physical response).

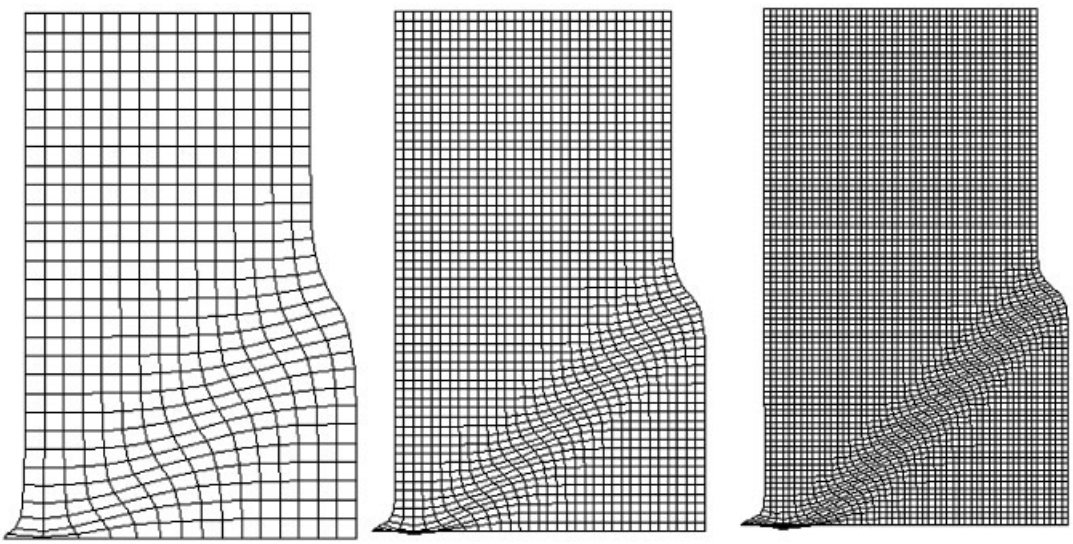

Figure 6. Mesh-independent results for 15×30, 30×60, and 45×90 meshes. Deformation patterns for gradient-dependent continuum with $\ell = 2.5$ mm (physical response: the width of the shear band is constant for different resolutions).

increase the width of the specimen towards the top, so that the shear band will be initiated at the bottom left and develops with an inclination angle of 45°, which is the analytical solution for a two-dimensional infinite medium under plane-strain condition [74].

First, the influence of geometrical non-linearity in the evolution of the shear band is investigated. In Figure 9(a) the displacement patterns for both meshes are plotted. We observe that the width of the shear band is determined by the element size by setting $\ell = 0$ (i.e. for classical strain-softening model). Deformation is localized along a line of integration points. Mesh dependence is also obvious from the effective plastic strain plots in Figure 9(b). When the mesh is refined, the dissipated energy decreases. Consequently, the inclusion of the geometrical non-linearity in the dissipation of the strain-softening material cannot solve the discretization dependence.

In order to solve the mesh-sensitivity problem, a length scale parameter of 2.5 mm is assumed in order to keep the field equations well-posed. In Figure 10(a), the displacement patterns are plotted. By comparison with the results of Figure 10(b), we observe that the shear band has a finite width which is almost independent of the finite element size. The inclination of the shear band is close to 45°. Also, similar distribution of the effective plastic strain contours can be observed from the two different meshes, which corroborates the mesh objectivity of results. Apparently, no visible discretization sensitivity is present in the results.

Because formulation of the gradient-dependent theory includes an internal length scale as a material parameter, numerical solutions employing a strain-softening model are no longer dependent on numerical discretization. However, one limitation to the discretization remains. The width of the localization zone needs to be many times (roughly 6) larger than the element size for proper calculation of the plastic strain.

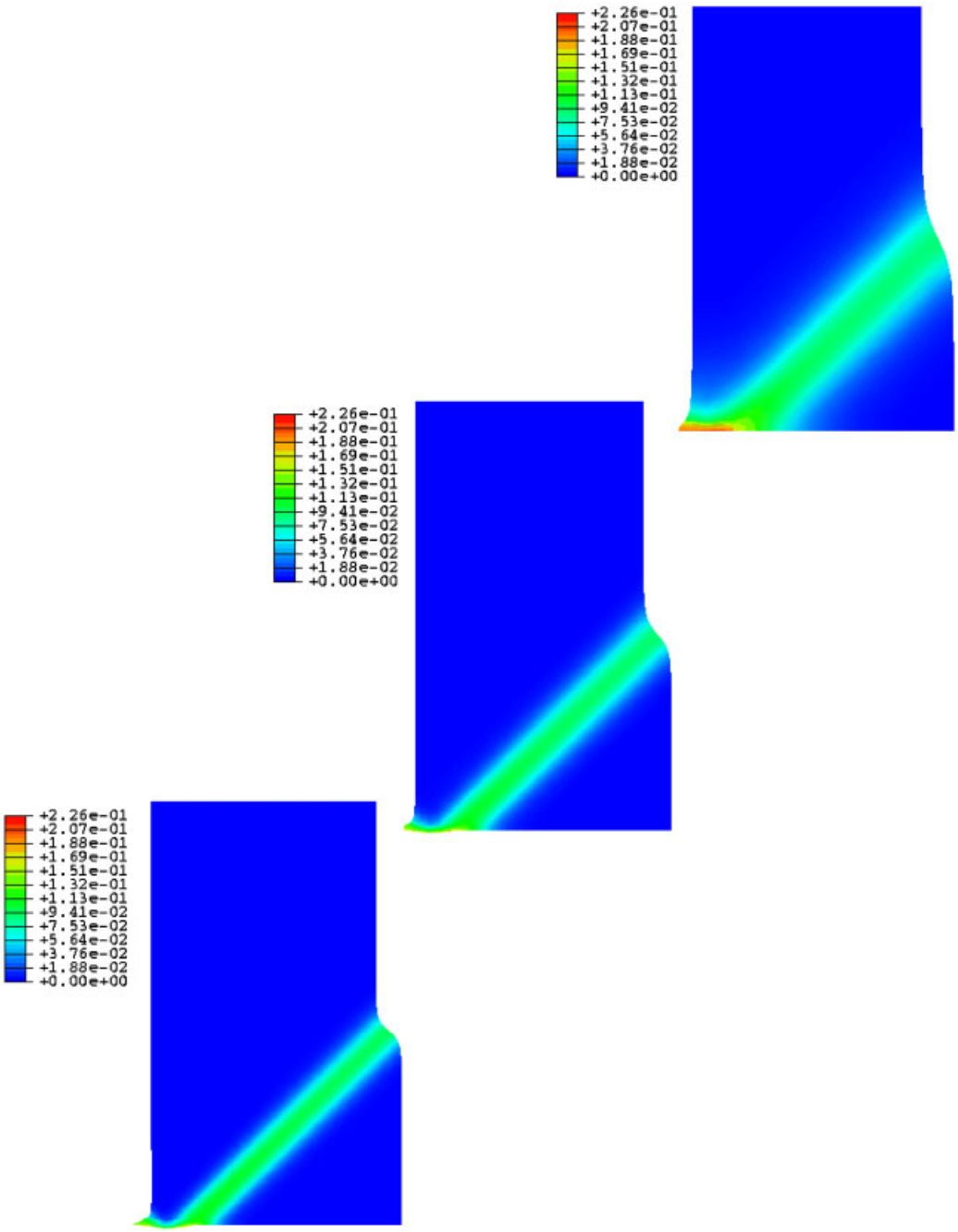

Figure 7. Mesh-sensitivity results for 15×30, 30×60, and 45×90 meshes. Mesh independent of effective plastic strain contours for gradient-dependent continuum with $\ell = 2.5$ mm (physical response).

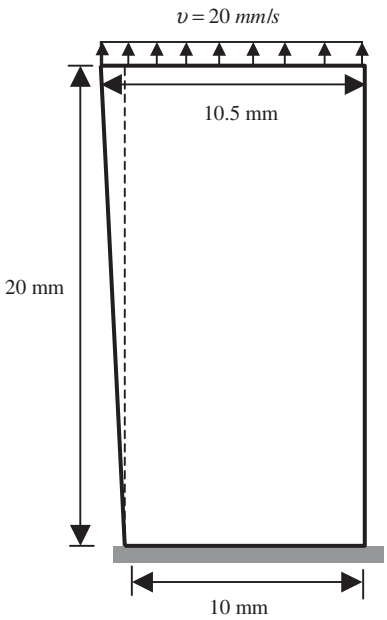

Figure 8. Strip in tension; problem description.

8. CONCLUSIONS

From the examples presented in this paper, introducing a material length scale in the classical continuum theory can preserve the well-posedeness of the governing equations and realistic responses are obtained. The numerical examples emphasize the regularization effect of the advocated gradient-dependent constitutive relations. The results converge to a unique solution upon mesh densification. Therefore, the mesh dependence exhibited by classical plasticity is remedied, allowing for robust localization and failure computations.

In order to avoid substantial modification of the procedure of the FEM implementation of a gradient-dependent model, the results of the gradient terms are obtained by a simple computational algorithm with little effort required to modify the normal FEM code. This approach provides high computational efficiency and no larger loss of precision compared to the normal FEM for general simple cases. Furthermore, the additional boundary conditions need to be applied only on the external boundary, avoiding the problem of tracking the internal elasto-plastic boundary. Consequently, the difficulty of enforcing additional boundary conditions in the de Borst approach with respect to the moving elasto-plastic boundary in the gradient theory is no longer present. In view of this, the usual displacement formulation for the finite element method is quite suitable for solving the (I)BVP of gradient inelasticity. The extension of this approach to three-dimensional finite elements is straightforward and can be generalized to more involved criteria than for the J2-flow materials. However, a disadvantage of this approach is that uniform mesh discretization is required, thus its application is limited. On the other hand, adapting this approach to meshless methods, i.e. element-free Galerkin method [75], that uses

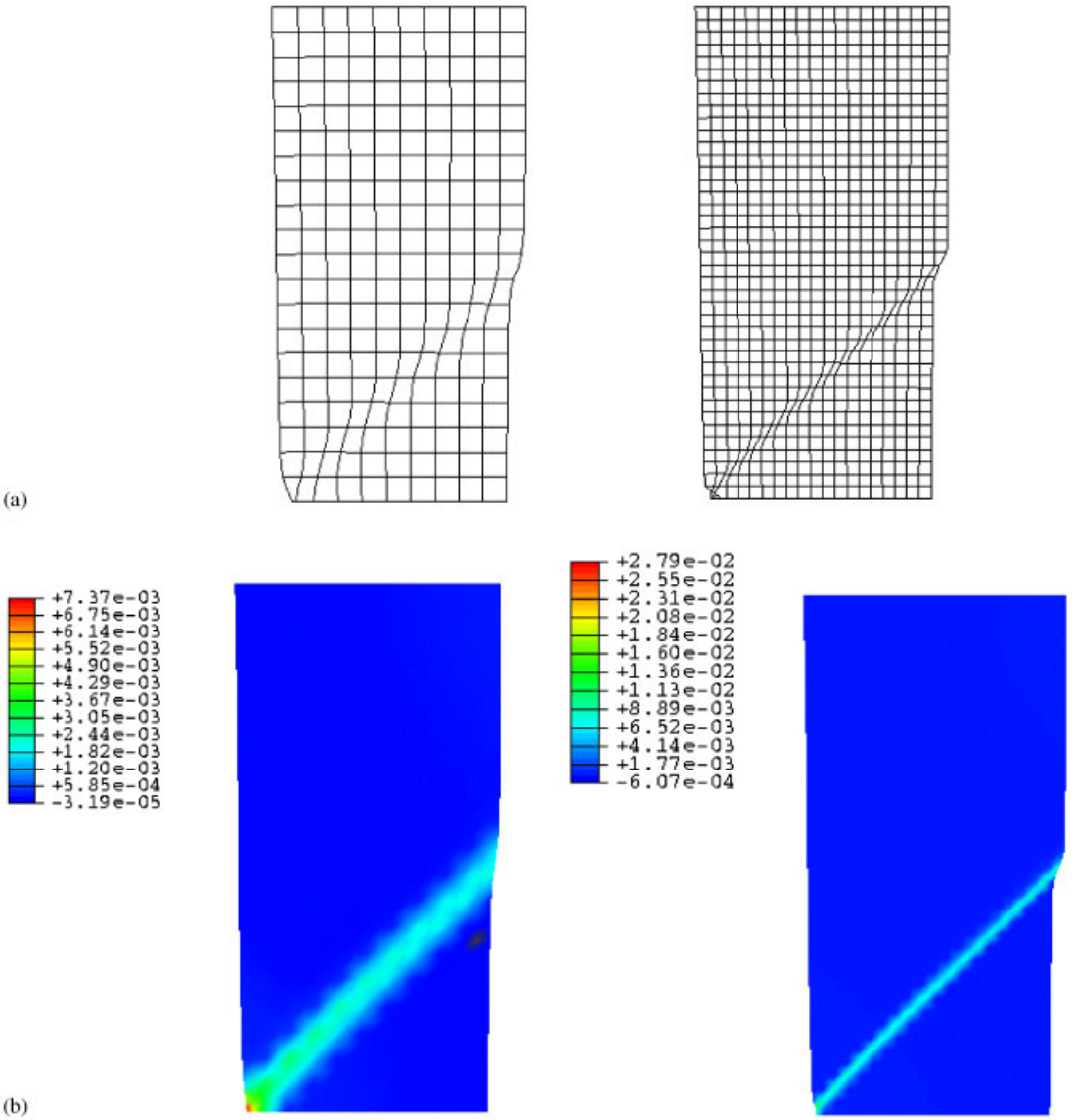

Figure 9. The mesh-dependent results when $\ell = 0$: (a) displacement patterns; and (b) the effective plastic strain contours.

gradient-dependent model could be advantageous and work in this direction is recommended. More elaborate work is also needed to extend this approach to non-regular meshes.

Numerical examples of two-dimensional biaxial test and strip in tension were presented, showing that using this finite element algorithm the mesh dependence of strain localization is removed. The determined shear band has expected inclination and reasonable thickness.

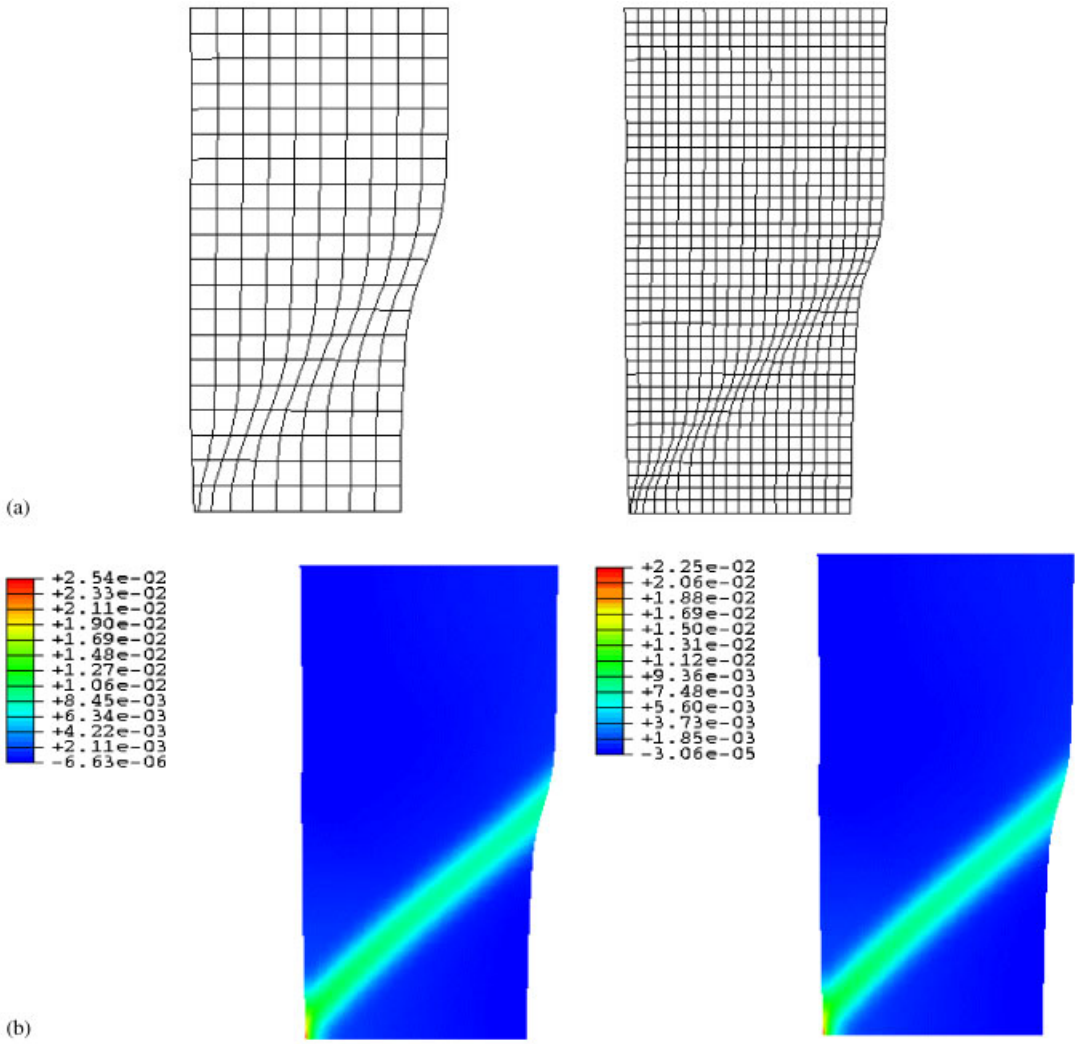

Figure 10. The mesh-independent results when $\ell = 2.5$: (a) displacement patterns; and (b) the effective plastic strain contours.

However, if the element size is significantly larger that the shear band width, the computational results are then affected by the mesh size.

ACKNOWLEDGEMENTS

The authors acknowledge the financial support under grant number M67854-03-M-6040 provided by the Marine Corps Systems Command, AFSS PGD, Quantico, Virginia. They thankfully acknowledge their appreciation to Howard 'Skip' Bayes, Project Director. The authors also acknowledge the financial

support under grant number F33601-01-P-0343 provided by the Air Force Institute of Technology, WPAFB, Ohio.

REFERENCES

1. Lasry D, Belytschko T. Localization limiters in transient problems. *International Journal of Solids and Structures* 1988; **24**:581–597.
2. de Borst R, Mühlhaus H-B. Gradient-dependent plasticity formulation and algorithmic aspects. *International Journal for Numerical Methods in Engineering* 1992; **35**:521–539.
3. de Borst R, Sluys LJ, Mühlhaus H-B, Pamin J. Fundamental issues in finite element analysis of localization of deformation. *Engineering Computations* 1993; **10**:99–121.
4. Pamin J. Gradient-dependent plasticity in numerical simulation of localization phenomena. *Dissertation*, Delft University of Technology, 1994.
5. de Borst R, Pamin J. Some novel developments in finite element procedures for gradient-dependent plasticity. *International Journal for Numerical Methods in Engineering* 1996; **39**:2477–2505.
6. Comi C, Perego U. A generalized variable formulation for gradient dependent softening plasticity. *International Journal for Numerical Methods in Engineering* 1996; **39**:3731–3755.
7. Ramaswamy S, Aravas N. Finite element implementation of gradient plasticity models. Part I: gradient-dependent yield functions. *Computer Methods in Applied Mechanics and Engineering* 1998; **163**:11–32.
8. Ramaswamy S, Aravas N. Finite element implementation of gradient plasticity models. Part II: gradient-dependent evolution equations. *Computer Methods in Applied Mechanics and Engineering* 1998; **163**: 33–53.
9. de Borst R, Pamin J, Geers M. On coupled gradient-dependent plasticity and damage theories with a view to localization. *European Journal of Mechanics – A/Solids* 1999; **18**:939–962.
10. Svedberg T, Runesson K. An adaptive finite element algorithm for gradient theory of plasticity with coupling to damage. *International Journal of Solids and Structures* 2000; **37**:7481–7499.
11. Kroner E. Dislocations and continuum mechanics. *Applied Mechanics Review* 1962; **15**:599–606.
12. Ashby MF. The deformation of plastically non-homogenous alloys. *Philosophy Magazine* 1970; **21**:399–424.
13. Eringen AC, Edelen DGB. On non-local elasticity. *International Journal of Engineering Science* 1972; **10**: 233–248.
14. Pijaudier-Cabot TGP, Bazant ZP. Nonlocal damage theory. *Journal of Engineering Mechanics* (ASCE) 1987; **113**:1512–1533.
15. Bazant ZP, Pijaudier-Cobot TGP. Nonlocal continuum damage, localization instability and convergence. *Journal of Applied Mechanics* 1988; **55**:287–293.
16. Aifantis EC. On the microstructural origin of certain inelastic models. *Journal of Engineering Materials and Technology* 1984; **106**:326–330.
17. Aifantis EC. The physics of plastic deformation. *International Journal of Plasticity* 1987; **3**:211–247.
18. Aifantis EC. On the role of gradients in the localization of deformation and fracture. *International Journal of Engineering Science* 1992; **30**:1279–1299.
19. Zbib HM, Aifantis EC. On the gradient-dependent theory of plasticity and shear banding. *Acta Mechanica* 1992; **92**:209–225.
20. Wang WM, Askes H, Sluys LJ. Gradient viscoplastic modeling of material instabilities in metals. *Metals and Materials-Korea* 1998; **4**:537–542.
21. Aifantis EC, Oka F, Yashima A, Adachi T. Instability of gradient dependent elastoviscoplasticity for clay. *International Journal for Numerical and Analytical Methods in Geomechanics* 1999; **23**:973–994.
22. Bammann DJ, Mosher D, Hughes DA, Moody NR, Dawson PR. Using spatial gradients to model localization phenomena. *Sandia National Laboratories Report*, *SAND99-8588*, Albuquerque, New Mexico 87185, Livermore, CA, 1999.
23. Ganghoffer JF, Sluys LJ, de Borst R. A reappraisal of non-local mechanics. *European Journal of Mechanics – A/Solids* 1999; **18**:17–46.
24. Oka F, Yashima A, Sawada K, Aifantis EC. Instability of gradient-dependent elastoviscoplastic model for clay and strain localization analysis. *Computer Methods in Applied Mechanics and Engineering* 2000; **183**:67–86.
25. Askes H, Pamin J, de Borst R. Dispersion analysis and element-free Galerkin solutions of second- and fourth-order gradient enhanced damage models. *International Journal for Numerical Methods in Engineering* 2000; **49**:811–832.

26. Kuhl E, Ramm E, de Borst R. An anisotropic gradient damage model for quasi-brittle materials. *Computer Methods in Applied Mechanics and Engineering* 2000; **183**:87–103.
27. Geers MGD, Peerlings RHJ, Brekelmans WAM, de Borst R. Phenomenological nonlocal approaches based on implicit gradient-enhanced damage. *Acta Mechanica* 2000; **144**:1–15.
28. Chen SH, Wang TC. Interface crack problem with strain gradient effects. *International Journal of Fracture* 2002; **117**:25–37.
29. Di Prisco C, Imposimato S, Aifantis EC. A visco-plastic constitutive model for granular soils modified according to non-local and gradient approaches. *International Journal for Numerical and Analytical Methods in Geomechanics* 2002; **26**:121–138.
30. Askes H, Sluys LJ. Explicit and implicit gradient series in damage mechanics. *European Journal of Mechanics – A/Solids* 2002; **21**:379–390.
31. Fremond M, Nedjar B. Damage, gradient of damage and principle of virtual power. *International Journal of Solids and Structures* 1996; **33**:1083–1103.
32. Voyiadjis GZ, Deliktas B, Aifantis EC. Multiscale analysis of multiple damage mechanics coupled with inelastic behavior of composite materials. *Journal of Engineering Mechanics* 2001; **127**:636–645.
33. Voyiadjis GZ, Abu Al-Rub RK, Palazotto AN. Non-local coupling of viscoplasticity and anisotropic viscodamage for impact problems using the gradient theory. *Archives of Mechanics* 2003; **55**:39–89.
34. Voyiadjis GZ, Abu Al-Rub RK, Palazotto AN. Thermodynamic formulations for non-local coupling of viscoplasticity and anisotropic viscodamage for dynamic localization problems using gradient theory. *International Journal of Plasticity* 2004; **20**:981–1038.
35. Gurtin ME. On a framework for small-deformation viscoplasticity: free energy, microforces, strain gradients. *International Journal of Plasticity* 2003; **19**:47–90.
36. Saczuk J, Hackl K, Stumpf H. Rate theory of nonlocal gradient damage-gradient viscoinelasticity. *International Journal of Plasticity* 2003; **19**:675–706.
37. Fleck NA, Hutchinson JW. A phenomenological theory for strain gradient effects in plasticity. *Journal of Mechanics and Physics of Solids* 1993; **41**:1825–1857.
38. Fleck NA, Muller GM, Ashby MF, Hutchinson JW. Strain gradient plasticity: theory and experiment. *Acta Metallurgica et Materialia* 1994; **42**:475–487.
39. Fleck NA, Hutchinson JW. Strain gradient plasticity. *Advances in Applied Mechanics* 1997; **33**:295–361.
40. Fleck NA, Hutchinson JW. A reformulation of strain gradient plasticity. *Journal of Mechanics and Physics of Solids* 2001; **49**:2245–2271.
41. Gao H, Huang Y, Nix WD, Hutchinson JW. Mechanism-based strain gradient plasticity—I. Theory. *Journal of Mechanics and Physics of Solids* 1999; **47**:1239–1263.
42. Gao H, Huang Y. Taylor-based nonlocal theory of plasticity. *International Journal of Solids and Structures* 2001; **38**:2615–2637.
43. Eringen AC. Theory of micropolar elasticity. In *Fracture*, *an Advanced Treatise*, Liebowitz H (ed.), vol. 2. Academic Press: New York, 1968; 621–729.
44. Mindlin RD. Micro-structure in linear elasticity. *Archives for Rational Mechanics and Analysis* 1964; **16**:51–78.
45. Cosserat E, Cosserat F. *Theorie des Corp Deformables*. Herman: Paris, 1909.
46. Abu Al-Rub RK. Material length scales in gradient-dependent plasticity/damage and size effects: theory and computation. *Doctoral Dissertation*, Louisiana State University, Louisiana, U.S.A., 2004.
47. Shu JY, Barrlow CY. Strain gradient effects on microscopic strain field in a metal matrix composite. *International Journal of Plasticity* 2000; **16**:563–591.
48. Busso EP, Meissonnier FT, O'Dowd NP. Gradient-dependent deformation of two-phase single crystals. *Journal of Mechanics and Physics of Solids* 2000; **48**:2333–2361.
49. Bassani JL. Incompatibility and a simple gradient theory of plasticity. *Journal of Mechanics and Physics of Solids* 2001; **49**:1983–1996.
50. Xue Z, Huang Y, Li M. Particle size effect in metallic materials: a study by the theory of mechanism-based strain gradient plasticity. *Acta Materialia* 2002; **50**:149–160.
51. Nix WD, Gao H. Indentation size effects in crystalline materials: a law for strain gradient plasticity. *Journal of Mechanics and Physics of Solids* 1998; **46**:411–425.
52. Shu JY, Fleck NA. The prediction of a size effect in micro-indentation. *International Journal of Solids and Structures* 1998; **35**:1363–1383.
53. Begley MR, Hutchinson JW. The mechanics of size-dependent indentation. *Journal of Mechanics and Physics of Solids* 1998; **46**:2049–2068.

54. Gao H, Huang Y, Nix WD. Modeling plasticity at the micrometer scale. *Naturwissenschaften* 1999; **86**: 507–515.
55. Huang Y, Gao H, Nix WD, Hutchinson JW. Mechanism-based strain gradient plasticity—II analysis. *Journal of Mechanics and Physics of Solids* 2000; **48**:99–128.
56. Huang Y, Xue Z, Gao H, Xia ZC. A study of micro-indentation hardness tests by mechanism-based strain gradient plasticity. *Journal of Material Research* 2000; **15**:1786–1796.
57. Yuan H, Chen J. Identification of the intrinsic material length in gradient plasticity theory from micro-indentation tests. *International Journal of Solids and Structures* 2001; **38**:8171–8187.
58. Swadener JG, George EP, Pharr GM. The correlation of the indentation size effect measured with indenters of various shapes. *Journal of Mechanics and Physics of Solids* 2002; **50**:681–694.
59. Abu Al-Rub RK, Voyiadjis GZ. Analytical and experimental determination of the material intrinsic length scale of strain gradient plasticity theory from micro- and nano-indentation experiments. *International Journal of Plasticity* 2004; **20**:1139–1182.
60. Abu Al-Rub RK, Voyiadjis GZ. Determination of the material intrinsic length scale of gradient plasticity theory. *International Journal of Multiscale Computational Engineering* 2004; **2**(3):47–70.
61. Aifantis EC. Strain gradient interpretation of size effects. *International Journal of Fracture* 1999; **95**: 299–314.
62. Tsagrakis I, Aifantis EC. Recent developments in gradient plasticity—Part I: formulation and size effects. *ASME Transactions*, *Journal of Engineering Materials and Technology* 2002; **124**:352–357.
63. Voyiadjis GZ, Abu Al-Rub RK. Gradient plasticity theory with variable length scale parameter. *International Journal of Solids and Structures*, submitted.
64. Peerlings RHJ, de Borst R, Brekelmans WAM, de Vree JHP. Gradient enhanced damage for quasi-brittle materials. *International Journal for Numerical Methods in Engineering* 1996; **39**:3391–3403.
65. Pamin J, Askes H, de Borst R. Two gradient plasticity theories discretized with the element-free Galerkin method. *Computer Methods in Applied Mechanics and Engineering* 2003; **192**:2377–2403.
66. Voyiadjis GZ, Dorgan RJ. Gradient formulation in coupled damage-plasticity. *Archives of Mechanics* 2001; **53**:565–597.
67. Mikkelsen LP. Post-necking behavior modeling by a gradient dependent plasticity theory. *International Journal of Solids and Structures* 1997; **34**:4531–4546.
68. Zervos A, Papanastasious P, Vardoulakis I. A finite element displacement formulation for gradient elastoplasticity. *International Journal for Numerical Methods in Engineering* 2001; **50**:1369–1388.
69. Nedjar B. Elastoplastic-damage modeling including the gradient of damage: formulation and computational aspects. *International Journal of Solids and Structures* 2001; **38**:5421–5451.
70. Chen J, Yuan H. A micro-mechanical damage model based on gradient plasticity: algorithms and applications. *International Journal for Numerical Methods in Engineering* 2002; **54**:399–420.
71. Liebe T, Menzel A, Steinmann P. Theory and numerics of geometrically non-linear gradient plasticity. *International Journal of Engineering Science* 2003; **41**:1603–1629.
72. Matsushima T, Chambon R, Caillerie D. Large strain finite element analysis of a local second gradient model: application to localization. *International Journal for Numerical Methods in Engineering* 2002; **54**: 499–521.
73. ABAQUS. *User Manual*, *Version 6.3*. Hibbitt, Karlsson and Sorensen, Inc.: Providence, RI, 2003.
74. Sluys LJ. Wave propagation, localization and dispersion in softening solids. *Ph.D. Thesis*, Delft University of Technology, The Netherlands, 1992.
75. Belytschko T, Lu YY, Gu L. Element-free Galerkin methods. *International Journal for Numerical Methods in Engineering* 1994; **37**:229–256.

